DNA condensation and redissolution: interaction between overcharged DNA molecules

2005 J. Phys.: Condens. Matter 17 S1827

(http://iopscience.iop.org/0953-8984/17/20/012)

INSTITUTE OF PHYSICS PUBLISHING JOURNAL OF PHYSICS: CONDENSED MATTER

J. Phys.: Condens. Matter **17** (2005) S1827–S1840 doi:10.1088/0953-8984/17/20/012

DNA condensation and redissolution: interaction between overcharged DNA molecules

Elshad Allahyarov[1,2,3,4], **Gerhard Gompper**[2] **and Hartmut Löwen**[1]

[1] Institut für Theoretische Physik II, Heinrich-Heine-Universität Düsseldorf, D-40225 Düsseldorf, Germany
[2] Institut für Festkörperforschung, Forschungszentrum Jülich, D-52425 Jülich, Germany
[3] Institute for High Temperatures, Russian Academy of Sciences, Izhorskaya 13/19, 117419 Moscow, Russia

E-mail: allahyar@thphy.uni-duesseldorf.de

Received 12 December 2004, in final form 21 January 2005
Published 6 May 2005
Online at stacks.iop.org/JPhysCM/17/S1827

Abstract

The effective DNA–DNA interaction force is calculated by computer simulations with explicit tetravalent counterions and monovalent salt. For overcharged DNA molecules, the interaction force shows a double-minimum structure. The positions and depths of these minima are regulated by the counterion density in the bulk. Using two-dimensional lattice sums and free energy perturbation theories, the coexisting phases for DNA bundles are calculated. A DNA condensation and redissolution transition and a stable mesocrystal with an intermediate lattice constant for high counterion concentration are obtained.

(Some figures in this article are in colour only in the electronic version)

1. Introduction

Long DNA is naturally found in a dense form in most biological systems due to the presence of compacting agents. *In vitro* the most used agents are polyamines such as trivalent spermidine (Spd) and tetravalent spermine (Spe) [1]. These agents play a key role in maintaining cellular DNA in a compact state [2, 3], modulate ion channel activities of cells, are essential for normal cell growth [4] and can effectively be applied in gene delivery and in the field of genetic therapy. Under physiologic ionic and pH conditions, the polyamines are positively charged and hence DNA is their prime target of interaction. The molecular mechanism of polyamine function in DNA condensation is presumed to involve neutralization of the negatively charged DNA backbone by the positively charged amino groups of Spd and Spe [5]. Experimental results and counterion condensation theories indicate that non-specific interactions are predominantly

[4] Author to whom any correspondence should be addressed.

electrostatic between polyamines and DNA phosphates [6–9]. Thus, the electrostatic shielding of phosphates facilitates close helix–helix surface contacts and, ultimately, DNA condensation through the correlation attraction [10], the attraction between strongly correlated counterion layers on the adjacent DNA surfaces.

In the last decade, different experiments [3, 11–16] have shown evidence of DNA redissolution (i.e. DNA unbinding) with increasing concentration of polyamines and several of their structural analogues. First, the addition of a certain amount of multivalent salt causes the collapse of single DNA or bundling in multi-columnar structures. Upon the addition of more salt, the polyelectrolyte redissolves and DNA assumes again an unbundled conformation. There are three experimentally well established features of the redissolution phenomena:

(i) a linear relationship is found between the threshold concentration of multivalent ions C_c, when the onset of DNA condensation takes place, and the initial DNA concentration c_{DNA} (the DNA concentration in solution free of multivalent ions);
(ii) the decondensation threshold C_d of multivalent ions, when the condensed DNA returns back to solution, is almost independent of monovalent salt concentration c_s;
(iii) between the threshold values C_c and C_d the DNA fragments show two coexisting liquid crystalline phases.

Concerning the first item, the onset of DNA condensation is usually explained by the correlation attraction between almost neutral structures. Thus, the precipitation induced by trivalent or tetravalent ions is not a consequence of the intrinsic structure and flexibility of DNA, but is a common feature of a polyelectrolyte solution. The threshold value C_c grows with increasing monovalent salt concentration c_s [2, 17–19]. A mono-molecular DNA collapse into a neutral toroidal structure occurs in highly dilute solutions of long DNA chains [3, 9], whereas a multi-molecular aggregation is generally observed in more concentrated DNA solutions, regardless of the DNA length [20, 21]. The second item, the DNA redissolution at C_d, is currently under intensive debate in the colloidal community with different, and sometimes conflicting, explanations [12, 13, 16, 17, 22]. For instance, in [12] it is argued that after precipitation the increased binding of polyamines will make the DNA hydrophilic enough to dissolve in water. Other experiments [22] show that the DNA is still in a condensed state when polyions are added beyond the threshold concentration C_d, but it is more finely dispersed in the solution. In [17] the reentrance is explained by resorting to DNA overcharging phenomena, which take place roughly in the middle of the condensation plateau. DNA is claimed to experience negative electrophoresis and move opposite to the conventional direction near the reentrance transition. However, experiments of Raspaud *et al* [9] do not confirm this claim. In [13] it was suggested that the redissolution is very sensitive to the relationship between the condensation of multivalent counterions on the polyelectrolyte and multivalent counterion–monovalent coion association (Bjerrum pairs). Thus, if the chemical potential of the multivalent counterions is low, they more likely adsorb on the DNA and overcharge it. On the other hand, if the chemical potential is high, the counterion–coion associations are more likely to appear in solution. A resulting condensation of Bjerrum pairs creates consecutive layers of oppositely charged ions around the DNA molecule [14, 23].

While the first two above-mentioned items have been studied in considerable detail, much less attention has been paid to the third item, namely the coexistence of two different liquid-like structures in DNA condensates. In a series of experiments, Livolant and colleagues demonstrated that the spermidine and spermine ions are capable of provoking several liquid crystalline forms of fragmented DNA [11]. Similar results were published recently by Saminathan *et al* in [3].

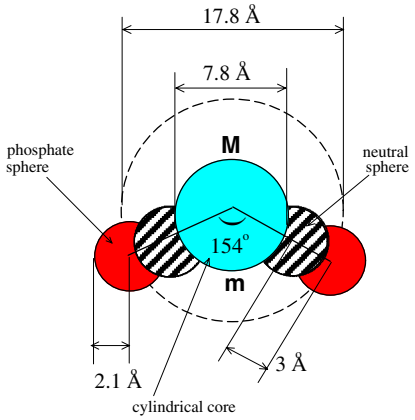

Figure 1. Cross section of DNA in the xy plane for the Montoro–Abascal model (MAM). Phosphate charges are shown as dark spheres. The DNA cylindrical core is coloured in grey, the hatched areas correspond to neutral hard spheres. The inscribed letters 'M' and 'm' denote the major and minor grooves correspondingly.

In this paper we investigate the condensation and redissolution of DNA on a molecular level by using computer simulations of the primitive-model electrolyte with explicit tetravalent counterions and monovalent salt ions. We trace back the condensation and redissolution to the distance-dependent effective potential $U(R)$ between two parallel DNA molecules, where R is the radial distance between their two centres. Using two-dimensional liquid-state theory for the fluid and lattice sums for the solid phases, we calculate the phase diagram for columnar DNA assemblies. A previous account of the results was already published elsewhere [28].

The remainder of this paper is organized as follows. In section 2 we describe our model system and give the definition of DNA–DNA interaction forces. We calculate the interaction forces for different counterion and salt concentrations in section 3. Section 4 is devoted to the free energy perturbation theory for defining the liquid–liquid coexistence densities. We conclude in section 5.

2. The model

We consider a B-DNA molecule which is a double helix with a pitch length $P = 34$ Å. There are $N_p = 20$ phosphate charges for one helical turn, which makes one elementary charge for each 1.7 Å of axial rise. The geometrical shape and charge distribution of DNA is modelled through the accurate Montoro–Abascal model (MAM) [24, 25]. Its cross section is illustrated in figure 1.

A pair of DNA molecules are placed along the xy diagonal of a cubic simulation box of volume $V = L^3$. The size of the simulation box $L = 102$ Å corresponds to three full turns of DNA. The box also consists of N_Q multivalent ions with valency q_Q, $N_- = N_{s-} + q_Q N_Q$ monovalent coions and $N_+ = N_{s+} + N_c$ monovalent counterions. Here $N_{s+} = N_{s-} = N_s$ is the number of added salt ion pairs, N_c is fixed by the DNA phosphate charge due to the constraint of global charge neutrality ($N_c = 120$ in our simulations). All ions are modelled as charged hard spheres. Tetravalent counterions are assumed to represent spermine ions. Though the latter is a polyion *in vivo*, a spherical approximation can be used, since the bibliographical data support the idea that it is the charge of counterion, rather than its structural specificities, which is important in DNA condensation and redissolution processes [9]. Besides this, the fluidity

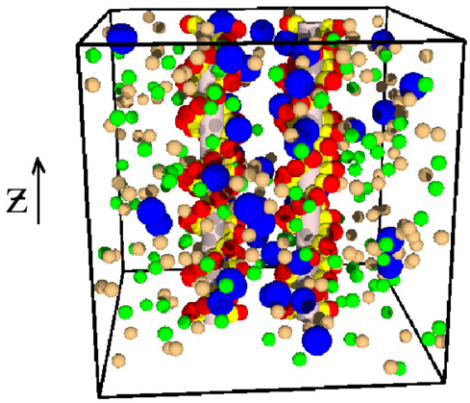

Figure 2. Typical snapshot in the simulation cell. The DNA molecules are shown as two parallel rods in the z direction, over-wrapped by two strings of light grey (neutral sphere in MAM (see text), coloured yellow in the online figure) and grey (phosphate sphere in MAM, red in the online figure) spheres. The tetravalent Spe ions are shown as big black (blue in the online figure) spheres. Light grey (yellow in the online figure) spheres represent coions, and dark grey (green in the online figure) spheres are monovalent counterions.

of the ordered DNA phase also suggests that spermine binds like an ordinary ion to the DNA surface, rather than forming inter-strand cross-links to neighbouring DNA molecules [11, 12]. Assuming that the ions of the same valency are indistinguishable, the actual number of mobile ion species in the simulation box is reduced from five (which are multivalent ions and their coions, positive and negative monovalent salt ions and monovalent counterions that neutralize the DNA phosphate charge) to three: multivalent counterions (charge $q_Q = 4$ and diameter d_Q) and positive and negative small ions (charge $q_c = \pm 1$ and diameter d_c). Periodic boundary conditions in all three directions are applied to reduce finite size effects. The DNA replicas in the z direction produce infinitely long molecules. The whole system is held at room temperature $T = 298$ K and the water is modelled as a continuous dielectric medium with dielectric constant $\epsilon = 80$. A typical snapshot of the simulation is shown in figure 2.

The interaction potentials between the five sort of particles (three of them are the mobile ions in solution mentioned above, and two of them, one charged and the other neutral, belong to the DNA molecule; see figure 1) are a combination of hard core and Coulomb potentials:

$$V_{ij}(r) = \begin{cases} \infty & \text{for } r \leqslant (d_i + d_j)/2 \\ \dfrac{q_i q_j e^2}{\epsilon r} & \text{for } r > (d_i + d_j)/2. \end{cases} \tag{1}$$

Here r is the interparticle distance, $i, j = Q$ for multivalent counterions, c for small ions, p for phosphate charges and n for neutral spheres in the MAM (with $q_n = 0$). There is also an excluded volume potential V_i^0 between the DNA hard cylinder and the free ions $i, j = Q, c$.

The basic quantity of interest is the effective force per helical turn [26]

$$\vec{F} = \vec{F}_1 + \vec{F}_2 + \vec{F}_3 \tag{2}$$

between two DNA molecules. Here $\vec{F}_1$ is the direct Coulomb repulsion per helical turn of one DNA molecule as exerted from the phosphate groups of the other DNA. It does not depend on salt density and its calculation is straightforward [27]. The second term $\vec{F}_2$ in equation (2) corresponds to Coulomb interactions between the phosphate charges at positions

$\vec{r}_k^{\,p}$ $(k = 1, \ldots N_\mathrm{p})$ and the mobile ions at positions $\vec{r}_l^{\,i}$ $(l = 1, \ldots, N_i, i = c, Q)$,

$$\vec{F}_2 = -\tfrac{1}{3}\sum_{k=1}^{3N_\mathrm{p}} \left(\left\langle \sum_{i=c,Q} \sum_{l=1}^{N_i} \vec{\nabla}_{\vec{r}_k^{\,p}} V_{pi}(|\,\vec{r}_k^{\,p} - \vec{r}_l^{\,i}\,|) \right\rangle \right). \tag{3}$$

Here $\langle \cdots \rangle$ denotes a canonical average over small ion configurations. The third term $\vec{F}_3$ in equation (2) arises from the entropic contribution of small ions due to their moment transform to the DNA surface $\mathcal{S}$,

$$\vec{F}_3 = -\tfrac{1}{3} k_\mathrm{B} T \int_{\mathcal{S}} \mathrm{d}\vec{f} \left(\sum_{j=c,Q} \langle \rho_j(\vec{r}) \rangle \right). \tag{4}$$

Here $\vec{f}$ is a surface normal vector pointing outwards from the DNA core and ρ_j $(j = c, Q)$ is the inhomogeneous microion concentration. The canonical averages in $\vec{F}_2$ and $\vec{F}_3$ are carried out over all configurations of the mobile ions.

We have performed extensive grand-canonical molecular dynamics (GCMD) simulations, similar to those of [27], for a range of different tetravalent counterion and monovalent salt concentrations. Each simulation is referred to by its nominal tetravalent counterion concentration C (salt ion concentration c_s) defined as a ratio between the total number of ions N_Q (N_s) in the cell without the DNA molecules and the system volume V, $C = N_Q/V$ $(c_\mathrm{s} = N_\mathrm{s}/V)$. Additional simulations have been carried out for these bulk phases in order to calculate the chemical potential μ of the solution. Then in the simulations with DNA molecules the number of ions in the simulation cell was automatically adjusted to the specified value of the chemical potential μ. The ion diameter was chosen to be $d_Q = 8$ Å for tetravalent counterions and $d_\mathrm{c} = 4$ Å for other free ions in the system. This parameter defines the closest approach of the ion to the DNA surface and has a strong impact on the polyion electrostatics. The time step $\triangle t$ of the simulation corresponds to an average ion displacement of 0.03 Å per time step such that the reflection of counterions following the collision with the combined surface of DNA is calculated with high precision. About 5×10^4 MD steps are required on average to reach equilibrium. The time evolution is then followed for 5×10^4–5×10^6 steps to gather statistics to calculate canonical averages of the interaction forces.

3. Results for the interaction forces

The case of a single DNA molecule in the presence of spermine ions has been considered in [28]. It was shown there (see figure 2 in [28]) that the ionic cloud may not only compensate the polyion charge but even exceed it, resulting in an opposite sign of the electrostatic potential at some distance from the DNA surface. The adsorption of Bjerrum pairs [23] onto the DNA surface at high tetravalent counterion concentration creates consecutive layers of charges of different sign around the DNA molecule. The onset of a multilayer structure occurs at $C = 1.8$ mM. Addition of monovalent salt shifts this threshold concentration to lower values of C, in accordance with experimental observations and two-component Manning condensation theory [29]. For multivalent counterion concentrations exceeding $C = 1.8$ mM, the total charge in the DNA grooves remains constant and only the total ionic charge adsorbed on the strands contributes to the overcharging, similar to our earlier findings [25, 28]. Besides this, there is a competition between the multivalent and monovalent counterions in binding to the DNA surface as C increases. The multivalent ions tend to replace the monovalent counterions on the DNA surface. Thus, at higher C the main contribution to the formation of charged layers around DNA molecules comes from Bjerrum association between big counterions and small coions. Such charged layers give rise to an attraction between two parallel DNA molecules, as

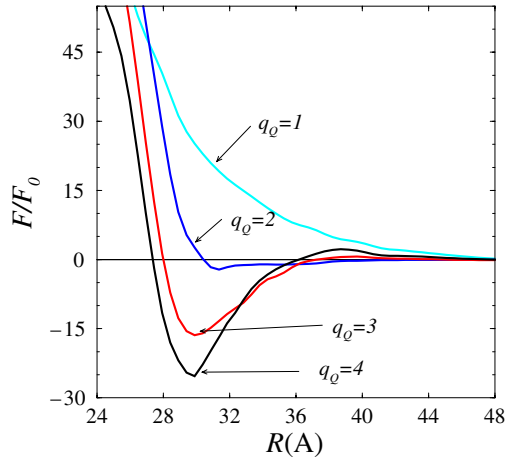

Figure 3. DNA–DNA interaction force F/F_0 versus intermolecular separation distance R for $c_s = 25$ mM and $C = 65$ mM. The charge of the big counterions is indicated next to the corresponding curves. $F_0 = k_B T/P$, where $P = 34$ Å.

shown in figure 3. A decrease of the big counterion charge leads to the break-up of the Bjerrum counterion–coion pairs and thus destroys the layer formation around the DNA molecule. This ultimately results in the loss of intermolecular attraction; see simulation data for $q_Q = 1, 2$ and 3 in figure 3.

It should be mentioned that in addition to the intermolecular (or axis-to-axis) distance R, there are angular variables which define the mutual configuration of two parallel DNA molecules corresponding to the orientation of their grooves and strands [26]. At short surface-to-surface distances between the two DNA molecules up to 5 Å there are strong contributions from particular DNA–DNA configurations [27]. For larger separation distance, $R > 25$ Å, we find no detectable dependence of the interaction forces on the mutual orientations of DNA molecules. On the other hand, there is experimental evidence that in DNA condensates two neighbouring molecules never approach each other more closely than 5 Å. This apparently means that at such small distances a strong repulsion between DNA solvation shells exists. Thus in all figures hereafter we show orientationally averaged interaction forces starting from the distance $R = 24$ Å. The interaction forces are scaled per DNA pitch, i.e. per 10 DNA base pairs.

The electrostatic F_2 and entropic F_3 components of total interaction force F for tetravalent counterions corresponding to DNA overcharging are separately plotted in figure 4. It can be seen that the electrostatic force shows oscillations around zero, which are reminiscent of the multilayered structure of charges around a single DNA molecule [28]. The deep attractive minimum of the total force F has an entropic origin, whereas the second minimum at intermolecular distance $R = 41$ Å has a purely electrostatic origin.

In figure 5 we plot the DNA–DNA interaction force for both the undercharged and overcharged cases at different salt concentrations. It is evident that in dense salt solutions the attractive minimum becomes weaker. For overcharged DNA, $C = 65$ mM, the position of the second minimum shifts towards the DNA surface. Thus, whereas the DNA overcharging does not strongly depend on the added salt concentration c_s [28], the effective forces do.

The positions of the minimum and the maximum of the force shift towards the DNA surface also for higher spermine concentrations. This trend is shown in figure 6, where the

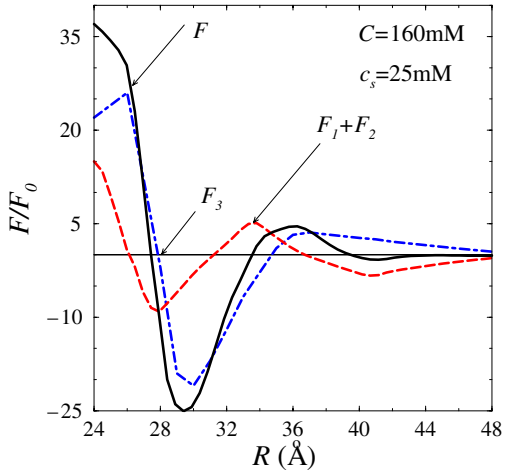

Figure 4. DNA–DNA interaction force F/F_0 versus intermolecular separation distance R for $c_s = 25$ mM, $C = 160$ mM. $F_0 = k_BT/P$, where $P = 34$ Å. The parameters correspond to complete DNA overcharging. Note that there is a second maximum in the total force F at about $R = 36$ Å and a second minimum at about $R = 41$ Å.

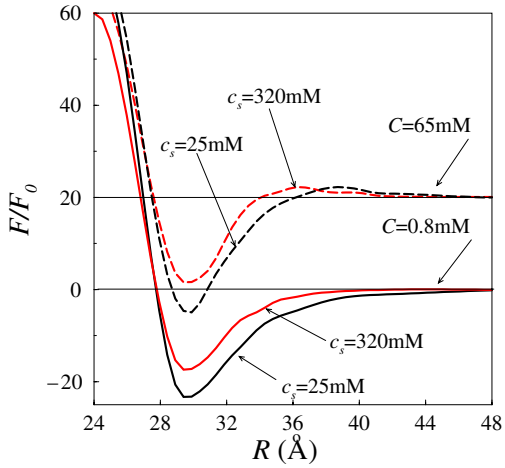

Figure 5. DNA–DNA interaction force versus intermolecular separation distance R for $c_s = 25$ mM (black lines in the online figure) and $c_s = 320$ mM (red lines in the online figure) and two different spermine concentrations: $C = 0.8$ mM (undercharged DNA, solid lines) and $C = 65$ mM (overcharged DNA, dashed lines). $F_0 = k_BT/P$, where $P = 34$ Å. The curves that correspond to $C = 65$ mM are shifted upward for clarity.

DNA–DNA interaction force is plotted for different spermine and salt concentrations at fixed distance $R = 38$ Å. For low C, which in figure 6 corresponds to the area to the left of point A, the DNA–DNA interaction is overall repulsive. Between points A and B a first minimum develops in F. As the spermine concentration increases further, the minimum shifts toward the DNA surface and the force has a repulsive tail. This tail indicates the appearance of second maximum, which obviously is followed by second minimum.

The dependence of the DNA–DNA interaction force on C for two fixed intermolecular distances is shown in figure 7. The five different arrows in this picture point to different

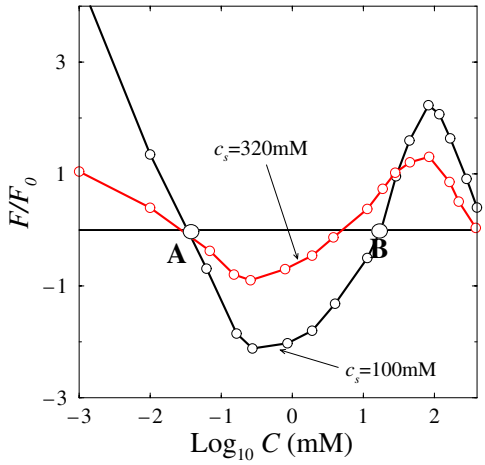

Figure 6. DNA–DNA interaction force versus spermine concentration C. The intermolecular separation distance is $R = 38$ Å (roughly the position of the second maximum for $C = 65$ mM). In the region between points A and B (for salt concentration $c_s = 100$ mM) a first minimum of the interaction force develops. $F_0 = k_B T/P$, where $P = 34$ Å.

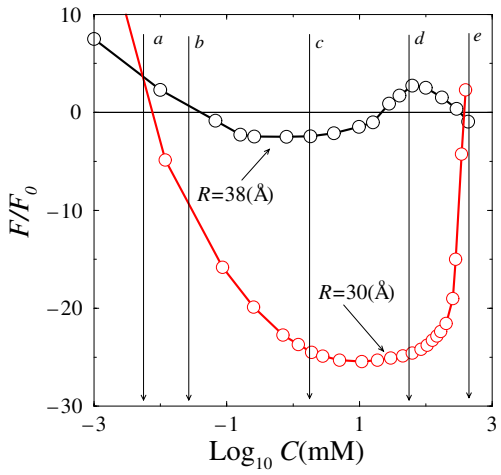

Figure 7. DNA–DNA interaction force versus spermine concentration C at fixed intermolecular separation distances R for $c_s = 25$ mM. At $R = 30$ Å ($R = 38$ Å) the first (second) minimum emerges at intermediate spermine concentrations C and then disappears at higher C. The arrows and labels (*a* to *e*) next to them are a guide to the eyes to point out the different spermine concentrations where the shape of the interaction force undergoes significant changes. For more details see the text.

values of C which characterize the number of attractive minima in the interaction force F. For small $C = 0.01$ mM, indicated by the arrow next to *a* in figure 7, the interaction force has no minimum and thus is totally repulsive. For spermine concentration $C = 0.025$ mM, corresponding to the arrow next to *b*, the force has a single minimum. For intermediate $C = 1.7$ mM and $C = 56$ mM, see the arrows next to *c* and *d* respectively, there are two minima in the interaction force (note that a positive force at $R = 38$ Å for C corresponding

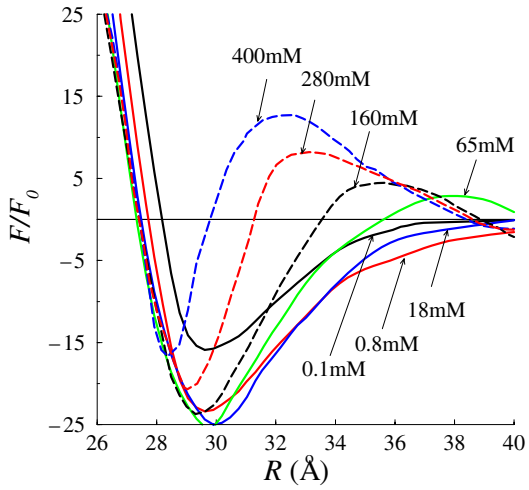

Figure 8. DNA–DNA interaction force versus intermolecular separation distance R for c_s = 25 mM, Different spermine concentrations are indicated next to the corresponding curves: $C = 0.1$, 0.8, 18, 65, 160, 280, 400 mM. $F_0 = k_B T/P$, where $P = 34$ Å is the DNA pitch length.

to arrow d indicates the occurrence of a second maximum, which obviously is followed by a second minimum at larger R). And finally, at even higher $C = 400$ mM, the first minimum has disappeared; however, the second minimum is retained.

A full set of distance-resolved DNA–DNA interaction force curves for different tetravalent counterion densities C is presented in figure 8. It can be seen that even a small trace of spermine ions—well below the overcharging threshold—induces an attraction between the DNA molecules, except at very close distances; see the curve for $C = 0.1$ mM. As the DNA molecules get more overcharged, which corresponds to high spermine concentrations, the main minimum narrows and becomes more shallow. At the same time, the width and the height of the maximum increase. We note that the attractive minimum for an undercharged DNA pair has mainly a pure electrostatic origin and arises due to charge correlations in the electrolyte. However, for overcharged DNA the main contribution to the force at this minimum is due to the spermine crowding near the DNA surface. The second maximum originates both from electrostatic and entropic forces. Finally, the second minimum emerges from a pure electrostatic effect.

In the following we calculate the total effective pair interaction potential $U(R)$ per unit length for a given bulk salt concentration c_s and different Spe concentrations C. The quantity $U(R)$ is obtained by integrating the distance-resolved interaction force averaged over all microion configurations [33]. Results are shown in figure 9. The oscillations in the force imply that the interaction potential also oscillates. With increasing C, the first minimum of $U(R)$ becomes deeper and it achieves a maximal depth at the overcharging concentration $C \approx 1.8$ mM. A further increase of C again reduces the depth of this minimum. The position of the minimum, on the other hand, hardly depends on C. The Spe-layering around the pair of DNA molecules induces a second minimum at larger separations as revealed in the enlarging inset of figure 9. This minimum is of electrostatic origin and occurs for $C \geqslant 65$ mM. Again the depth of the second minimum first increases and then decreases with increasing C. At intermediate Spe concentrations, we are thus confronted with a double minimum potential which is induced by layering. It is worth mentioning that the positions of the second minimum

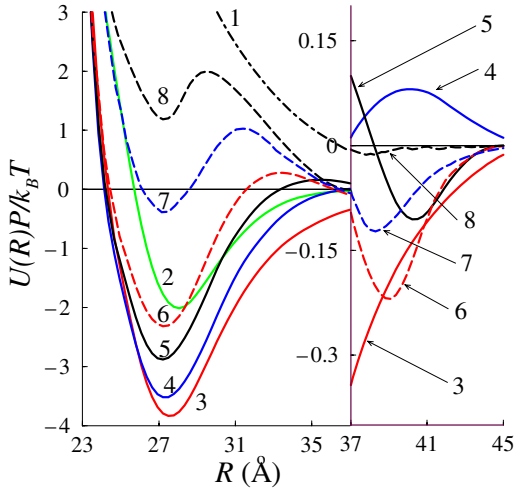

Figure 9. DNA–DNA effective pair potential versus intermolecular separation distance R for $c_s = 25$ mM. The spermine concentrations are $C = 0$ mM (1), 0.1 mM (2), 0.8 mM (3), 18 mM (4), 65 mM (5), 160 mM (6), 280 mM (7), 400 mM (8).

can be related to intermolecular distances between the DNA molecules in the cholesteric phase induced by polyamines [32, 3]. Direct measurements [30] and theoretical investigations [31] of intermolecular forces demonstrated that the energetics of this cholesteric phase is determined primarily by electrostatic interactions. Since the potentials in figure 9 are scaled for one DNA pitch length, the interaction strength corresponding to the minimum of curve (2) for very long DNA molecules is sufficiently large to induce condensation. This implies that DNA aggregation can take place well *below* overcharging Spe concentrations.

4. Phase diagram for double-minimum potential

The characteristic double-minimum structure of the interaction potential $U(R)$ will give rise to an unusual phase behaviour. We have calculated the phase diagram of a columnar DNA assembly on the basis of our simulated effective pair interactions. To do so, we assume that the DNA molecules are parallel along a certain length ℓ. This length is an additional parameter which we fix to be $\ell = 20 \times P$. We comment on the dependence of the phase diagram on ℓ in section 5. The assembly of parallel DNA can be considered as a two-dimensional many-body system interacting via a potential $\ell \times U(R)$ and being characterized by a DNA particle number density ρ. We calculated the free energies of the fluid and solid phases by using different techniques outlined below and perform the traditional Maxwell double tangent construction to identify the coexisting densities.

The free energy of a dilute *fluid* phase is approximated by two-dimensional perturbation theory [34] via splitting the total potential into repulsive and attractive parts, $U(R) = U_r(R) + U_a(R)$. The repulsive potential $U_r(R)$, identical to $U(R)$ but truncated and shifted towards zero at the first minimum at $R = R_{min}$, is mapped onto that of effective hard discs of diameter σ_{eff} [35]

$$\sigma_{eff} = \sigma + \int_{\sigma}^{R_{min}} \left[1 - \exp\left(-\frac{U_r(R)}{k_B T}\right)\right] dR. \tag{5}$$

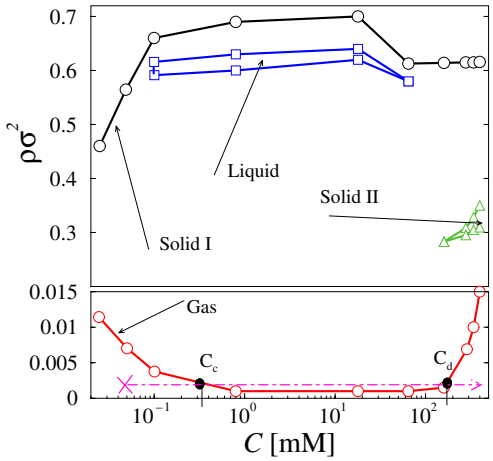

Figure 10. Coexisting DNA densities as a function of Spe concentrations C, for $c_s = 25$ mM. The stable phases found are gas-like, liquid and two triangular crystals with different lattice constants (solid I and solid II). All phase transitions between these phases are of first order. For the sake of better resolution at smaller DNA densities, the y-axis is expanded below $\rho\sigma^2 < 0.015$.

Here the cross-section diameter for the DNA molecule is $\sigma = 20$ Å. The total Helmholtz free energy involves that of a hard disc fluid with effective area fraction $\eta = \frac{\pi\rho\sigma_{\rm eff}^2}{4}$ and a mean-field correction which we simply model as $\pi\rho^2 \int_\sigma^\infty \frac{U_a(R)}{k_B T} R\,{\rm d}R$. For the free energy of a hard-disc fluid, analytical expressions are available [36]. The free energy of the *solid* phase, on the other hand, is calculated as a lattice sum with the assumption of a two-dimensional triangular lattice structure. The lattice constant is directly related to the DNA number density ρ.

Figure 10 shows the resulting phase diagram with the coexisting DNA densities for the wide range of C. At low C there is a strong first-order gas–crystal phase transition whose coexistence region is widened for larger C due to the increasing attractions. Between the two threshold concentrations $C \approx 0.1$ mM and $C \approx 65$ mM there is enough attraction to stabilize a liquid phase of high DNA density. At higher Spe concentrations a second crystal, with a considerably larger lattice constant than that of the high-density solid, emerges. We call this novel phase a mesocrystal since its density is intermediate between that of the fluid and the almost close-packed solid.

Condensation (see the cross in figure 10) and subsequent redissolution (dot–dashed line in figure 10) of dilute DNA solution are other implications of the phase diagram. As the spermine concentration increases for fixed $\rho\sigma^2 = 0.002$, which corresponds to a typical DNA concentration of 1 mg ml^{-1} DNA, first the gas–liquid coexistence line is encountered. This is the condensation transition and the system will split into a low density gas and a high density liquid phase. At much higher C the coexistence line is touched again and the system redissolves back into the dilute gas phase. The corresponding threshold concentrations of the condensation and redissolution are in the range $C_c \approx 0.3$ mM and $C_d \approx 165$ mM, and agree well with the experimental observations [9, 11].

5. Discussions and conclusions

One issue we want to discuss is the dependence of the phase diagram on the DNA length ℓ. Since ℓ is a prefactor of the effective potential, it plays formally the role of an inverse system

temperature. We have explored the phase behaviour for smaller and larger DNA segment lengths of $\ell = 5$ P and 100 P respectively. First, the stability of the liquid pocket depends sensitively on ℓ; it disappears completely for small ℓ, but extends towards larger C for larger ℓ. Second, the fluid coexistence density shifts to considerably higher values for smaller ℓ. Hence, condensation and redissolution are prohibited for small DNA segment lengths. This is in line with the experiments of [37], where a threshold value of $\ell \approx 15$ P for the minimal length ℓ required for condensation is reported. For a triplex DNA (three-stranded DNA molecule) the minimal length is reported to be about 2 P [37]. The difference between the minimal lengths for duplex and triplex DNA segments arises from the DNA charge density [38, 39]. The higher the linear charge density, the stronger the overcharging. This in turn results in the precipitation of triplex DNA at spermine concentrations, where duplex DNA does not aggregate [37, 12].

The DNA fragments considered here have a length less than the persistence length of the DNA molecule, which is around 500 Å. That is why one can safely adopt a rigid rod assumption for the DNA molecule and avoid the intramolecular fluctuations (off the long DNA axis). This is also in line with the experiments [11–16] where the DNA redissolution measurements were done for DNA segments which are smaller than the persistence length. Hence the particles involved are very stiff rods.

We speculate that the height of the energetical barrier between the two minima in the interaction potential $U(R)$ could regulate the DNA segment lengths in the crystalline structures observed in experiments. Imagine that the solution consists of a mixture of DNA segments of different lengths (but still smaller than the persistence length 500 Å). At lower spermine concentration, when the interaction potential has a single minimum, all DNA segments will form a bundle with an average interparticle distance of the order of $R = 28$ Å. However, when the energetical barrier develops at intermediate spermine concentrations with a height around 0.5–1 $k_{\mathrm{B}}T$ per pitch length, only a short DNA segment could overcome this repulsion. Thus, short segments will fall into the first minimum and form a dense hexagonal structure, while longer DNA segments will be trapped in the second minimum and form a more swollen, fluid-like structure, apparently a cholesteric phase.

The other issue is the orientational entropy of DNA molecules and its influence on the interaction potential and free energy of DNA solutions. The evaluation of the contribution to the free energy from the orientational entropy of two nonparallel DNA rods (intermolecular fluctuations) in MD simulations is a tremendous task. In fact, the DNA–DNA effective potential must be averaged over all possible orientations for two DNAs. Unfortunately, an implementation of tilted DNA molecules will break the system symmetry in simulations. On the other hand, simulation of 20 P long molecular segments for the system parameters invoked here still is a challenge. For the bundle phase, due to the deep attraction (more than 40 $k_{\mathrm{B}}T$) between the DNA rods of 20 P length, all other than parallel configurations of DNA molecules have little statistical weight. Thus, only a tiny correction to the energy of bundle is expected.

For the dilute gas phase the orientational entropy for DNA rod has an upper limit of about $2\,k_{\mathrm{B}}T$. At lower DNA densities, when the average DNA–DNA distance is of the order of or less than the DNA length, this entropy should be added to the free energy of liquid phase. On the length-scale of free energy, where both the liquid perturbation and lattice sum produced curves have deep minima about dozen $k_{\mathrm{B}}T$ at intermediate DNA densities, such an upward shift of liquid free energy at smaller DNA densities will have only a slight effect on the phase diagram for 20 P long DNA fragments. In other words, a corresponding upward shift of the free energy of a dilute DNA system will not strongly affect the coexistence spermine concentration values deduced from the double-tangent procedure. Hence, a length of 20 P for the DNA segment is enough to safely neglect orientational entropy effects in the phase diagram shown in figure 10.

In conclusion, we have calculated the influence of tetravalent counterions on the effective interactions and the phase diagram of columnar DNA assemblies by primitive-model-type computer simulations and statistical theories. We find that a small concentration of tetravalent counterions induces DNA condensation. The layering of the strongly coupled tetravalent counterions on the DNA strands yields an oscillatory effective interaction potential with a double-minimum structure at intermediate counterion concentrations. This explains the redissolution transition and triggers a novel stable mesosolid. Our threshold concentrations are in good agreement with experimental data.

Acknowledgment

We acknowledge a partial support of this work by the European Networks of Excellence 'SoftComp'.

References

[1] Cohen S S 1998 *A Guide to Polyamines* (New York: Oxford University Press)
[2] Bloomfield V A 1997 *Biopolymers* **44** 269
[3] Saminathan M, Thomas T, Shirahata A, Pillai C K S and Thomas T J 2002 *Nucleic Acids Res.* **30** 3722
[4] Cason A L *et al* 2003 *Eur. J. Hum. Genet.* **1** 8
[5] Wilson R W and Bloomfield V A 1979 *Biochemistry* **18** 2192
Wilson R W, Rau D C and Bloomfield V A 1980 *Biophys. J.* **30** 317
[6] Deng H, Bloomfield V A, Benevides J M and Thomas G J Jr 2000 *Nucleic Acids Res.* **28** 3379
[7] Braunlin W H, Anderson C F and Record M T Jr 1986 *Biopolymers* **25** 205
Braunlin W H and Xu Q 1992 *Biopolymers* **32** 1703
[8] Olvera de la Cruz M, Belloni L, Delsanti M, Dalbiez J P, Spalla O and Drifford M 1995 *J. Chem. Phys.* **103** 5781
[9] Raspaud E, Chaperon I, Leforestier A and Livolant F 1999 *Biophys. J.* **77** 1547
Raspaud E, Olvera M, de la Cruz M O, Sikorav J-L and Livolant F 1998 *Biophys. J.* **74** 381
[10] Stilck J F, Levin Y and Arenzon J J 2002 *J. Stat. Phys.* **106** 287
[11] Pelta J, Livolant F and Sikorav J-L 1996 *J. Biol. Chem.* **271** 5656
Pelta J, Durand D, Doucet J and Livolant F 1996 *Biophys. J.* **71** 48
[12] Saminathan M, Antony T, Shirahata A, Sigal L H, Thomas T and and Thomas T J 1999 *Biochemistry* **38** 3821
[13] Solis F J and De la Cruz M O 2001 *Eur. Phys.* E **4** 143
[14] Solis F J 2002 *J. Chem. Phys.* **117** 9009
[15] de Vries R 2001 *Biophys. J.* **80** 1186
[16] Murayama Y, Sakamaki Y and Sano M 2003 *Phys. Rev. Lett.* **90** 018102
[17] Nguyen T T, Rouzina I and Shklovskii B I 2000 *J. Chem. Phys.* **112** 2562
Nguyen T T and Shklovskii B I 2001 *J. Chem. Phys.* **115** 7298
[18] Bloomfield V A 1996 *Curr. Opin. Struct. Biol.* **6** 334
[19] Burak Y, Ariel G and Andelman D 2003 *Biophys. J.* **85** 2100
[20] Arscott P G, Li A-Z and Bloomfield V A 1990 *Biopolymers* **29** 619
[21] Solis F J and De la Cruz M O 2000 *J. Chem. Phys.* **112** 2030
[22] Trubetskoy V S, Wolff J A and Budker V G 2003 *Biophys. J.* **84** 1124
[23] Tanaka M and Grosberg A Yu 2001 *J. Chem. Phys.* **115** 567
[24] Montoro J C G and Abascal J L F 1995 *J. Chem. Phys.* **103** 8273
Montoro J C G and Abascal J L F 1998 *J. Chem. Phys.* **109** 6200
Abascal J L F and Montoro J C G 2001 *J. Chem. Phys.* **114** 4277
[25] Allahyarov E, Löwen H and Gompper G 2003 *Phys. Rev.* E **68** 061903
[26] Allahyarov E and Löwen H 2000 *Phys. Rev.* E **62** 5542
[27] Allahyarov E, Gompper G and Löwen H 2004 *Phys. Rev.* E **69** 041904
[28] Allahyarov E, Löwen H and Gompper G 2004 *Euro. Phys. Lett.* **68** 894
[29] Manning G S 1978 *Q. Rev. Biophys.* **11** 179
[30] Strey H H, Parsegian V A and Podgornik R 1999 *Phys. Rev.* E **59** 999
[31] Kornyshev A A and Leikin S 2000 *Phys. Rev. Lett.* **84** 2537

[32] Durand D, Doucet J and Livolant F 1992 *J. Physique* II **2** 1769
[33] Allahyarov E, D'Amico I and Löwen H 1998 *Phys. Rev. Lett.* **81** 1334
[34] Weeks J D, Chandler D and Andersen H C 1971 *J. Chem. Phys.* **54** 5237
[35] Evans R 1990 *Liquids at Interfaces* (Amsterdam: North-Holland)
[36] Santos A, Lopez de Haro M and Bravo Yuste S 1995 *J. Chem. Phys.* **103** 4622
[37] Goobes R, Cohen O and Minsly A 2002 *Nucleic Acids Res.* **30** 2154
[38] Deserno M, Jimenez-Angeles F, Holm C and Lozada-Cassou M 2003 *Preprint* cond-mat/0104002
[39] Deserno M, Jimenez-Angeles F, Holm C and Lozada-Cassou M 2001 *J. Phys. Chem.* B **105** 10983